*Geol. Mag.* **156** (*1*), *2019, pp. 117–132* © *Cambridge University Press 2017*
doi:10.1017/S0016756817000851


# Geology, biostratigraphy and carbon isotope chemostratigraphy of the Palaeogene fossil-bearing Dakhla sections, southwestern Moroccan Sahara

MOULOUD BENAMMI*†, SYLVAIN ADNET‡, LAURENT MARIVAUX‡, JOHAN YANS§, CORENTIN NOIRET§, RODOLPHE TABUCE‡, JÉRÔME SURAULT*, IMAD EL KATI¶, SÉBASTIEN ENAULT‡, LAHSSEN BAIDDER||, OMAR SADDIQI|| & MOHAMED BENAMMI¶

*Institut International de Paléoprimatologie, Paléontologie Humaine: Evolution et Paléoenvironnements (iPHEP), UMR-CNRS 7262, Université de Poitiers UFR SFA, 40 avenue du Recteur Pineau, F-86022 Poitiers cedex, France
‡Institut des Sciences de l'Evolution de Montpellier (ISE-M), UMR 5554 CNRS/UM/IRD/EPHE, CC064, Université de Montpellier, place Eugène Bataillon, F-34095 Montpellier cedex 05, France
§Department of Geology, University of Namur, rue de Bruxelles 61, 5000 Namur, Belgium
¶Laboratoire de Géologie, Géophysique, Géorisques et Environnement (3GE), Département de Géologie, Université Ibn Tofail, Faculté des Sciences, BP. 133, Kenitra, Morocco
||Laboratoire Géosciences, Université Hassan II-Casablanca, BP 5366 Maârif, Casablanca, Morocco

(*Received* 14 March 2017; *accepted* 11 September 2017)

**Abstract** – New Palaeogene vertebrate localities were recently reported in the southern Dakhla area (southwestern Morocco). The Eocene sediment strata crops out on cliffs along the Atlantic Ocean coast. Vertebrate remains come from five conglomeratic sandstone beds and are principally represented by isolated teeth belonging to micromammals, selachians and bony fishes, a proboscidean assigned to ?*Numidotherium* sp. and many remains of archaeocete whales (Basilosauridae). From fieldwork five lithostratigraphic sections were described, essentially based on the lithological characteristic of sediments. Despite the lateral variations of facies, correlations between these five sections were possible on the basis of fossil-bearing beds (A1, B1, B2, C1 and C2) and five lithological units were identified. The lower part of the section consists of rhythmically bedded, chert-rich marine siltstones and marls with thin black phosphorite with organic matter at the base. The overlying units include coarse-grained to microconglomeratic sandstones interbedded with silts, indicating deposition in a shallow-marine environment with fluvial influence. The natural remanence magnetization of a total of 50 samples was measured; the intensity of most of the samples is too weak however, before or after the first step of demagnetization. The palaeomagnetic data from the samples are very unstable, except for eight from three similar sandstone levels which show a normal polarity. Matched with biostratigraphic data on rodents, primates, the selachian, sirenian and cetacean faunas, the new carbon isotope chemostratigraphy on organics (1) refines the age of the uppermost C2 fossil-bearing bed to earliest Oligocene time and (2) confirms the Priabonian age of the B1 to C1 levels.

Keywords: Oligocene rodents, southwestern Morocco, magnetostratigraphy, chemostratigraphy, biostratigraphy

## 1. Introduction

The study area lies in the south of Morocco, 60 km south of the coastal town of Dakhla between the gulf of Cintra and N'Tireft village (Fig. 1), between latitudes 22° 50′ and 24° 5′ N, and forms part of the Tarfaya-Dakhla Basin. It is the southernmost Atlantic basin of Morocco, and extends from the Mauritania border in the south to the Canary Islands in the north. It stretches over more than 1000 km along the western margin of the Sahara and covers an area of 170,000 km$^2$, both on- and offshore (Davison, 2005; Sachse *et al*. 2011, 2014). The geological and stratigraphic structures of the basin have been investigated in detail using well and seismic data (Kolonic *et al*. 2002; Klingelhoefer *et al*. 2009; Davison & Dailly, 2010). The Tarfaya-Dakhla Basin is filled with Mesozoic and Cenozoic continental to shallow-marine sediments, which overlie the basement Precambrian and/or Palaeozoic rocks.

The escarpment exposes Palaeogene to Quaternary sediments, which have recently been noted for their abundant and diverse marine and terrestrial faunas, particularly vertebrates (Adnet, Cappetta & Tabuce, 2010; Benammi *et al.* 2014*a*, *b*; Zouhri *et al*. 2014; Marivaux *et al.* 2017*a*). Palaeontological data are also exploited by commercial fossil dealers and amateur fossil collectors, meaning that the site requires protection by the authorities as a geosite (Saddiqi *et al*. 2015).

This work, based on lithologic, palaeomagnetic, carbon isotope chemostratigraphy and biochronological data, allows us to describe and refine the nature and age of the sedimentological deposits exposed in the Dakhla

†Author for correspondence: mbenammi@univ-poitiers.fr

https://doi.org/10.1017/S0016756817000851 Published online by Cambridge University Press

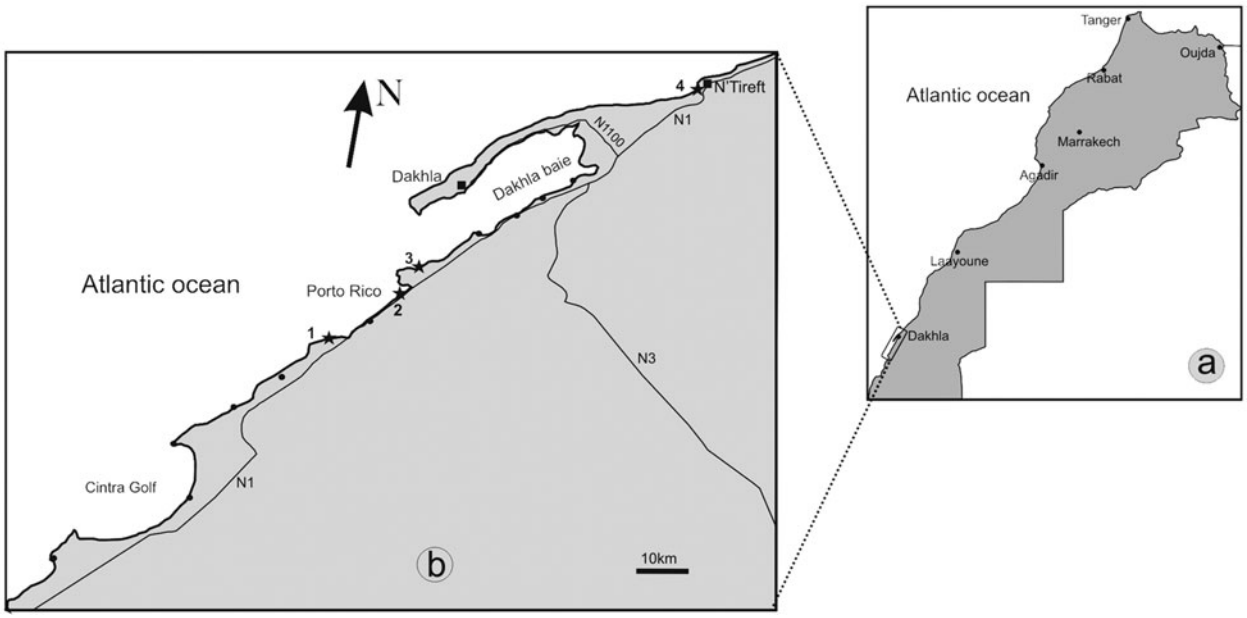


Figure 1. Geographic location of the Dakhla peninsula, south of Morocco. (a) Map of Morocco with principal towns and (b) location of the geological sections studied (stars). 1, Garitas; 2, Porto Rico; 3, El Argoub. The black circles represent the outcrops of interest along the Atlantic Ocean coast.

region, and to constrain the dating of its palaeontological content (Palaeogene faunas).

## 2. Geological setting

The studied Palaeogene succession corresponds to the Samlat Formation of Ratschiller (1967). It is exposed in different areas, notably cliffs along the Atlantic Ocean coast, and has also been recognized in borehole drillings (Ranke, Von Raad & Wissmann, 1982; Davison, 2005) on the continental shelf. There have been a few geological studies carried out on these units in the Dakhla area (e.g. Ratschiller, 1967; Ortlieb, 1975) which were inappropriately mapped as Mio-Pliocene by Rjimati *et al*. (2008), contrary to those studies on deposits capping the beach cliffs near Dakhla and dated to the Mio-Quaternary period (e.g. Joleaud, 1907; Front & Sague, 1911; Deperet, 1912; Lecointre 1962, 1966). In the framework of our geological and palaeontological program in the early Tertiary period of North Africa, since 2013 we have carried out fieldwork in the westernmost part of the Sahara in Morocco, notably on the geological outcrops of the Samlat Formation exposed between Garitas and about 60 km north of the crossroads at the entrance of the Dakhla peninsula (Fig. 1a, b). Recent palaeontological studies in this region have yielded vertebrate fossils, which indicate that some of the deposits are late Eocene in age (Adnet, Cappetta & Tabuce, 2010; Zouhri *et al*. 2014). New sedimentological, geochemical and magnetostratigraphic studies were carried out in order to refine the age of these Palaeogene deposits. Between 2013 and 2015, our field research was devoted to prospecting the outcrops in search of fossil-bearing levels. The escarpment prospected lies between latitudes 22° 51′ and 24° N (in some zones the outcrops are covered by modern sand dunes). About 150 km south of Dakhla, the thickness of the outcrops is reduced and is only a few metres above sea level. It is only from Garitas and beyond to the north that the escarpment exposes Palaeogene sediments, notable for their abundant and diverse marine vertebrates.

## 3. Materials and methods

In order to reconstruct the past sedimentary environment, outcrops were sought in the Dakhla peninsula and in the surrounding areas. For each outcrop, a number of sections were selected for detailed study along the coastal cliffs. The succession of lithofacies was described from the base to the top of the sequence for each section. The description was essentially based on the lithological characteristic of sediments and the sedimentary structures. This description enabled us to establish correlations between sections based on fossil-bearing levels as previously reported in Adnet, Cappetta & Tabuce (2010).

Field studies included the selection of different outcrops with easy access; we measured five stratigraphic sequences, bed by bed, with Jacob Staff. These sections are located *c.* 50 km south of Dakhla. In addition, a palaeomagnetic study was carried out along the Porto Rico section (Fig. 1). A total of 29 cores were drilled in the field from 13 distinct levels with a portable gasoline-powered drill, and oriented *in situ* with a magnetic compass. Most sites drilled correspond to Unit 2 and the lower part of Unit 3 (see following section). The lithology sampled includes sandstones, clays and silts.

Carbon isotope analyses were performed on 43 samples (Table 1) of the Porto Rico (Pto) and El

https://doi.org/10.1017/S0016756817000851 Published online by Cambridge University Press

Table 1. Sample labels, $CaCO_3$ content (%) and $\delta^{13}C_{org}$ values (‰, VPDB); NA–not analysed.

| Section | Label | $CaCO_3$ (%) | $\delta^{13}C_{org}$ (‰ VPDB) |
|---|---|---|---|
| Porto Rico section | PTO15-18 | 0.0 | −25.2 |
| | PTO15-17 | 0.0 | −23.7 |
| | PTO15-16 | 0.0 | −25.4 |
| | PTO15-15 | 0.0 | −24.7 |
| | PTO15-14 | 0.0 | −24.6 |
| | PTO15-13 | 0.0 | −23.9 |
| | PTO15-11 | 55.1 | −22.1 |
| | PTO15-10 | 1.0 | −22.5 |
| | PTO15-9 | 0.6 | −26.2 |
| | PTO15-8 | 5.0 | −24.6 |
| | PTO15-7 | 0.0 | −25.2 |
| | PTO15-5 | 0.0 | −24.6 |
| | PTO-41 | 2.0 | −25.6 |
| | PTO15-4 | 0.0 | −25.0 |
| | PTO15-3 | 0.0 | −25.8 |
| | PTO15-2 | 1.2 | −24.3 |
| | PTO-34 | 76.0 | −24.6 |
| | PTO15-1 | 76.9 | −24.3 |
| | PTO-32B | 1.0 | −24.4 |
| | PTO-30B | 1.0 | −25.1 |
| | PTO-26B | 1.0 | −24.9 |
| | PTO-22B | 2.0 | −25.0 |
| | PTO-21B | 59.0 | −25.1 |
| | PTO-16B | 60.0 | −25.7 |
| | PTO-2 | 43.0 | −27.6 |
| El Argoub section | ARG15-12 | 0.0 | −25.5 |
| | ARG15-11 | 0.0 | −25.4 |
| | ARG15-10 | 1.4 | −23.0 |
| | ARG15-9 | 1.3 | −25.7 |
| | ARG15-8 | 0.0 | −25.1 |
| | ARG15-7 | 1.0 | −25.0 |
| | ARG15-6 | 3.2 | −24.2 |
| | ARG15-4 | 45.3 | −24.5 |
| | ARG15-3 | 28.7 | −23.4 |
| | ARG15-2 | 0.0 | −27.8 |
| | ARG15-1 | 0.5 | −24.2 |
| Not analysed (TOC too low) | PTO15-12 | 41.2 | TOC too low |
| | PTO15-6 | 0.0 | TOC too low |
| | ARG15-5 | NA | TOC too low |
| | PTO-43 | 3.0 | TOC too low |
| | PTO-19 | NA | TOC too low |
| | PTO-11 | 19.0 | TOC too low |
| | PTO-5 | NA | TOC too low |

Argoub (Arg) sections. Organic matter of the sediments was isolated following the procedure described by Yans *et al*. (2010) and refined by Storme *et al*. (2012). The bulk organic carbon isotope analyses ($\delta^{13}C_{org}$) are based on powdered rock samples of *c.* 1–10 g, acidified in 25 % HCl solution for two hours in order to remove carbonate. The numerous carbonate-free samples were treated similarly. Soluble salts were removed by repetitive (1–10 times) centrifuging (4000 revolutions per minute) with deionized water until a neutral sediment was obtained. Finally, residues were dried at 35 °C and powdered again. Carbon isotope analysis of organic carbon was performed with an elemental analyser (Carlo-Erba 1110) connected online to a Thermo Finnigan Delta V Plus mass spectrometer at the University of Erlangen (Germany). Organic $^{13}C/^{12}C$ values were normalized to the international VPDB standard (Vienna Pee Dee Belemnite). Each sample was analysed 1–4 times; the accuracy and reproducibility of the analyses were checked by replicate analyses of international standards USGS40 and USGS41. The reproducibility of analyses is within 0.2 ‰ (1σ). The $CaCO_3$ (%) content of the samples was measured with a Bernard Calcimeter.

## 4. Description of lithological units

Ratschiller (1967) first reported a precise lithology of Cenozoic deposits in central and western Moroccan Sahara, and defined: the Izic Formation, ranging from the uppermost Miocene to Pliocene deposits; the transgressive upper Miocene Aaiun Formation (Laayoun area); and the Palaeogene Samlat Formation. Based primarily on foraminifera, Ratschiller (1967) subdivided the Samlat Formation into three members: the Morcba Member which mainly consists of continental sand deposits with some petrified woods, assigned an Oligocene – early Miocene age despite the lack of age evidence; the thick Guerran Member which is primarily a marine siliceous chalk, becoming more clastic further onshore, assigned an Eocene age on the basis of foraminifera; and the Itgui Member, which consists principally of marine limestones with flint levels and is dated as being of Paleocene age.

The studied deposits of the Dakhla area formally belong to the Samlat Formation, but considering that the lithology of each Ratschiller's Member was defined further north (near Aauinat Tartar, south of Boujdour), we decided to use lithological units without reference to Ratschiller's members.

In the Dakhla region, the escarpment lies 10–60 m above sea level and forms a west-facing cliff, steepening on the upper part but sloping gently at the base. The studied sections are directly along a steep cliff at the Atlantic coast exposed between the Gulf of Cintra and N'Tireft village (Fig. 1b). The Palaeogene formation is overlain by a 1–2 m thick lumachellic limestone which is of Mio-Pliocene age (e.g. Joleaud, 1907; Front & Sague, 1911; Deperet, 1912; Lecointre, 1966) and consists of: alternating marine limestones and marls, rich in organic matter at the base; alternating sandstones and marls, with intercalations of brown to black siliceous limestones at the middle interval; and sandy white marls at the top.

### 4.a. Garitas section

This section is directly exposed along the cliff located *c.* 15 km north of Imlili village, in a locality named Garitas which is located in a restricted military area. Lateral variations of facies are obvious, especially regarding strata thickness. We have divided these sequences into five lithological units (Units 1–5 or U1–U5).

*Unit 1* represents the lowermost part of the section (as in Adnet, Cappetta & Tabuce 2010), and is composed of a succession of four lithofacies (Fig. 2). (1) The first lithofacies is a rhythmic sequence that consists of grey–beige marl limestone to whitish surface, sometimes siliceous with splintery fracture. This

https://doi.org/10.1017/S0016756817000851 Published online by Cambridge University Press

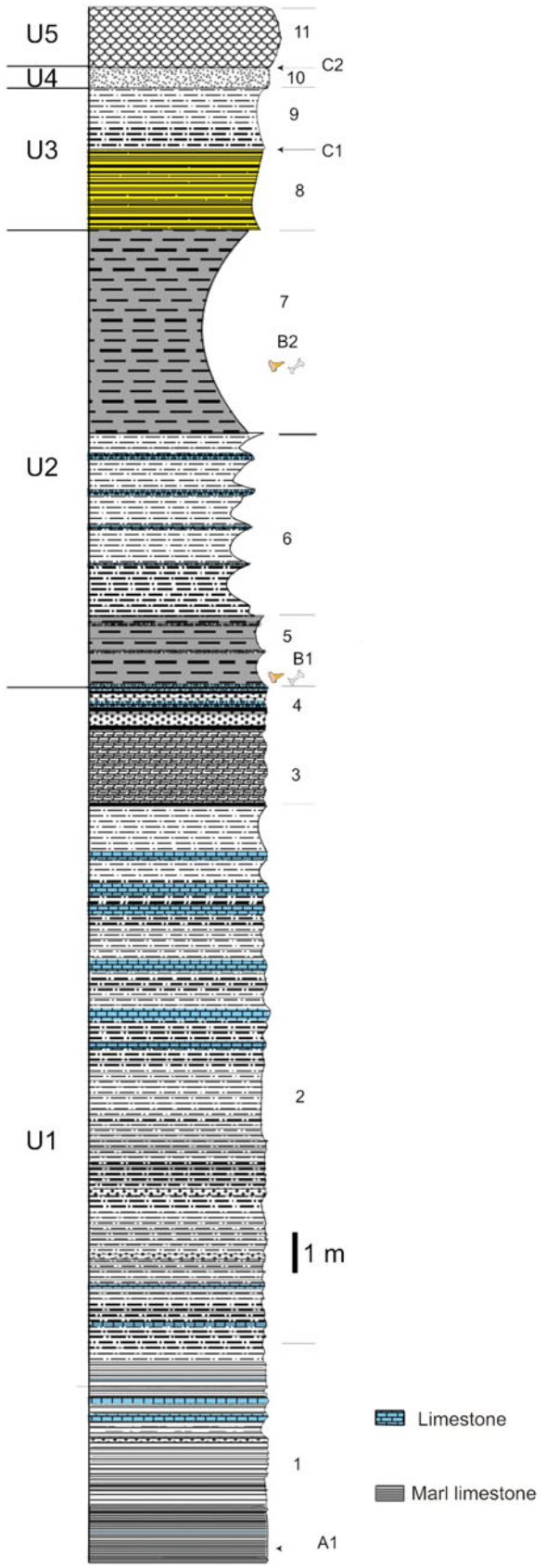


Figure 2. (Colour online) Stratigraphic section of the Garitas sedimentological sequence. U1–U5 refers to the unit, and the number on the right of the column represents the lithofacies.

marly limestone, showing sporadic black nodules, alternates with grey or blackish organic-matter-rich marl (Fig. 3a–c). The base of this sequence shows a *c.* 10 cm thick blackish phosphorite, rich in organic matter including numerous coprolites and fish remains (level A1, Fig. 3c). This latter level becomes thicker (20 cm thick) and whiter towards the south. (2) The second lithofacies is an alternating beige marl and siliceous limestone with vertical fissure filled with the same sediments (Neptunian dykes; Fig. 3e–f). The limestone beds show inverse graded bedding (decimetric at the bottom and multi-decimetric at the top). Several coprolite levels (Fig. 4a) are noted, of centimetre to decimetre thickness. (3) This level comprises compact grey limestone bars and beige sandy calcareous marl (Fig. 4b). (4) This landmark level is composed of black to brown or dark siliceous limestone, rich in coprolites at its base, and alternating with beige marls (Fig. 4b).

*Unit 2* is composed of two lithofacies. (5) Yellowish sandy marl (*c.* 1 m) is overlaid by a friable sandy micro-conglomeratic ferruginous level, which is particularly rich in selachian teeth and vertebrate bones (bed B1 of Adnet, Cappetta & Tabuce, 2010). This fossil-bearing level B1 (Fig. 4c) has yielded a large number of vertebrae of cetaceans belonging to five different species, with possible rib fragments of sirenians as well as a few remains of crocodiles, turtles, sea snakes and birds (Zouhri *et al*. 2014). (6) This whitish marl level includes intercalations of lenticular brown siliceous limestone (*c.* 5 m) (Figs 4b, 5a).

*Unit 3* comprises three lithofacies. (7) Muddy brown yellow sandstone, sometimes with a secondary gypsum element. This level yields abundant remains of selachians and archaeocetes (basilosaurids) (cf. Bed B2 of Adnet, Cappetta & Tabuce, 2010). Zouhri *et al*. (2014) reported a *Basilosaurus* sp. and remains of a dugongid from this level. (8) Fossil-rich beige sandy marl, yielding a few dental remains of terrestrial mammals (rodent incisor) and selachians (Level C1). (9) Beige sandy marls.

*Unit 4* includes lithofacies (10), composed of red sands (*c.* 0.5 m thickness).

*Unit 5* comprises lithofacies (11), a consolidated coquina deposit with oysters and gastropods (scallop bed of thickness *c.* 1.5 m).

#### 4.b. Porto Rico section

The section is located *c.* 10 km east of Dakhla city, along the shore of Porto Rico (Fig. 1b). In this area, the available section starts with the bone-bed fossil-bearing level B1 of U2 (Fig. 7), U1 being underwater (or perhaps absent?). From the bottom upwards, this section consists of units 2–4.

*Unit 2* comprises two lithofacies. (1) At the shoreline, the geological section begins with an oxidized sandy marl level rich in vertebrate bones and selachian teeth, corresponding to level B1 of Adnet, Cappetta & Tabuce (2010) (Fig. 7a). This very fossiliferous horizon lies on the previous section more

https://doi.org/10.1017/S0016756817000851 Published online by Cambridge University Press

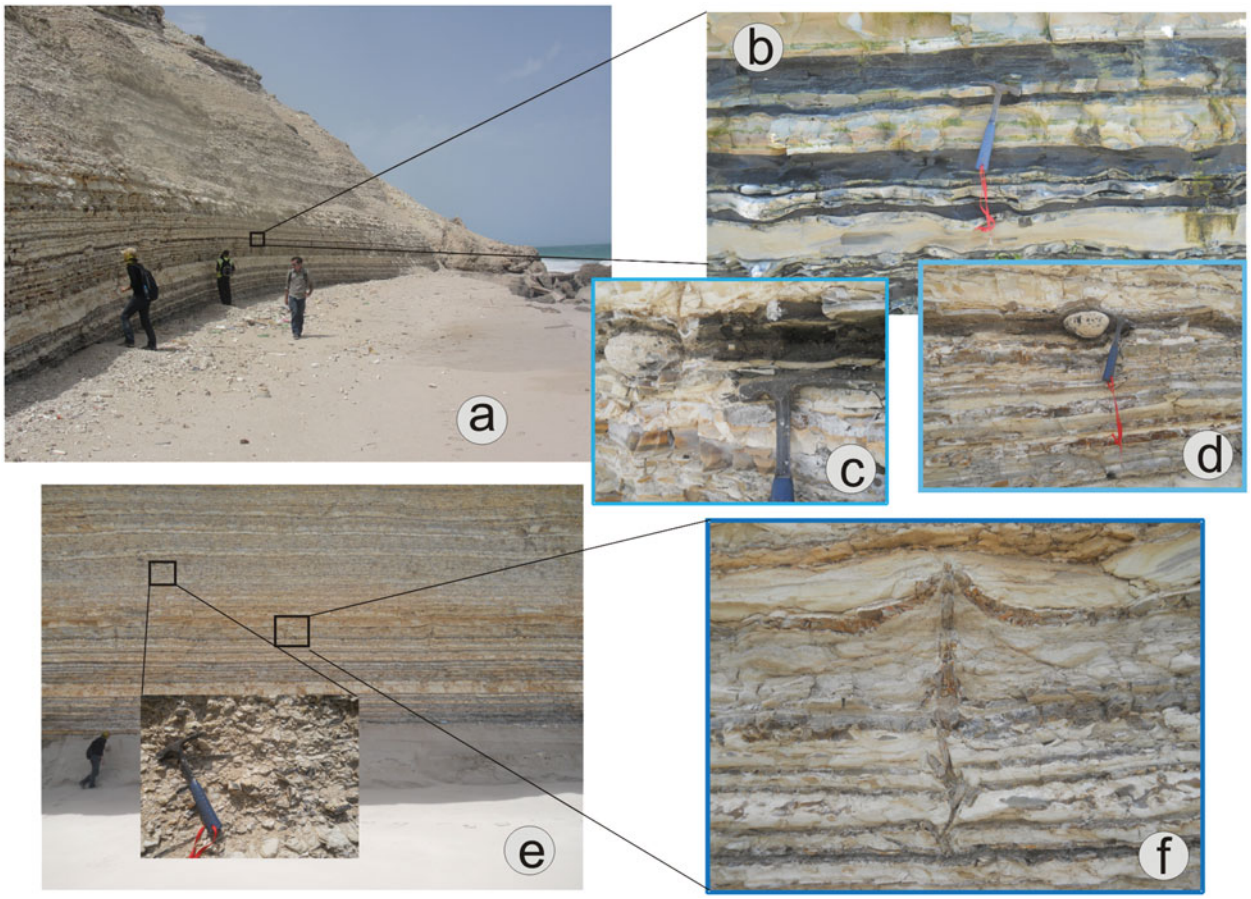


Figure 3. (Colour online) Field photographs showing: (a) a general view of the lower part of the Garitas section, horizontal heterolithic stratification; (b) a detail of (a), showing blackish sediments (A1) rich in organic matter levels; (c) a phosphorite-rich organic matter with shark teeth (fossil-bearing level A1); (d) black quartize nodule; (e) the beige marl and siliceous limestone; and (f) Neptunian dykes.

than 22 m above sea level and plunges northwards below sea level. (2) Beige to whitish sandy marls are topped by a yellowish and oxidized sandy marl level that is rich in fossils, the fossil-bearing level B2 of Adnet, Cappetta & Tabuce (2010) (Fig. 7c). These levels tend to disappear within a few hundred metres to the north of Porto Rico.

*Unit 3* comprises lithofacies (3). The middle of the section consists of a thick multicolour sandy marl series, interstratified by sandstone with limestone concretions. A rich level of selachian teeth and bones (Level C1) was identified in the lower part of this interval (Fig. 7b).

*Unit 4*, which is composed of lithofacies (4), begins with a very characteristic landmark level consisting of gastropod and oyster coquina (Fig. 7b, d) with white sandy marls in the middle. The fossil-bearing level C2 includes sandstone intercalations.

*Unit 5* ends the Porto Rico section with the Mio-Pliocene flagstone, consisting of a coquina limestone which includes oyster shells and gastropods (U5).

#### 4.c. North Porto Rico and El Argoub sections

These two sections are characterized by the development of both U3 and U4 units formed mainly by sandy marls, separated by the landmark gastropod coquina limestone (Fig. 8). Unit 4 shows green marls containing the fossiliferous level C2 at its base, red mudstones and laminated sandstones in the middle, and white sandy marls at the top. Unit 5 consists of a flagstone formed by laminated sandy limestones containing millimetric grains of quartz.

## 5. Correlation between the sections

The N–S logged sections were correlated based on (at least) five remarkable fossil-bearing levels (denoted A1, B1, B2, C1 and C2). In these measured sections, the lithostratigraphic units described in Section 4 above show lateral variations of facies along the coastline (Fig. 9). These variations can be explained by the slight northwards tilting of these deposits. The five units recognized represent a general regressive trend, which records a transition from an outer ramp into a peritidal zone. The rhythmic bedding might have been caused by fluctuations in the depositional environment.

With the exception of U5, the four units U1–4 are of Palaeogene age and therefore formally belong to the Samlat Formation. The correlations with the three members of the Samlat Formation of Ratschiller

https://doi.org/10.1017/S0016756817000851 Published online by Cambridge University Press

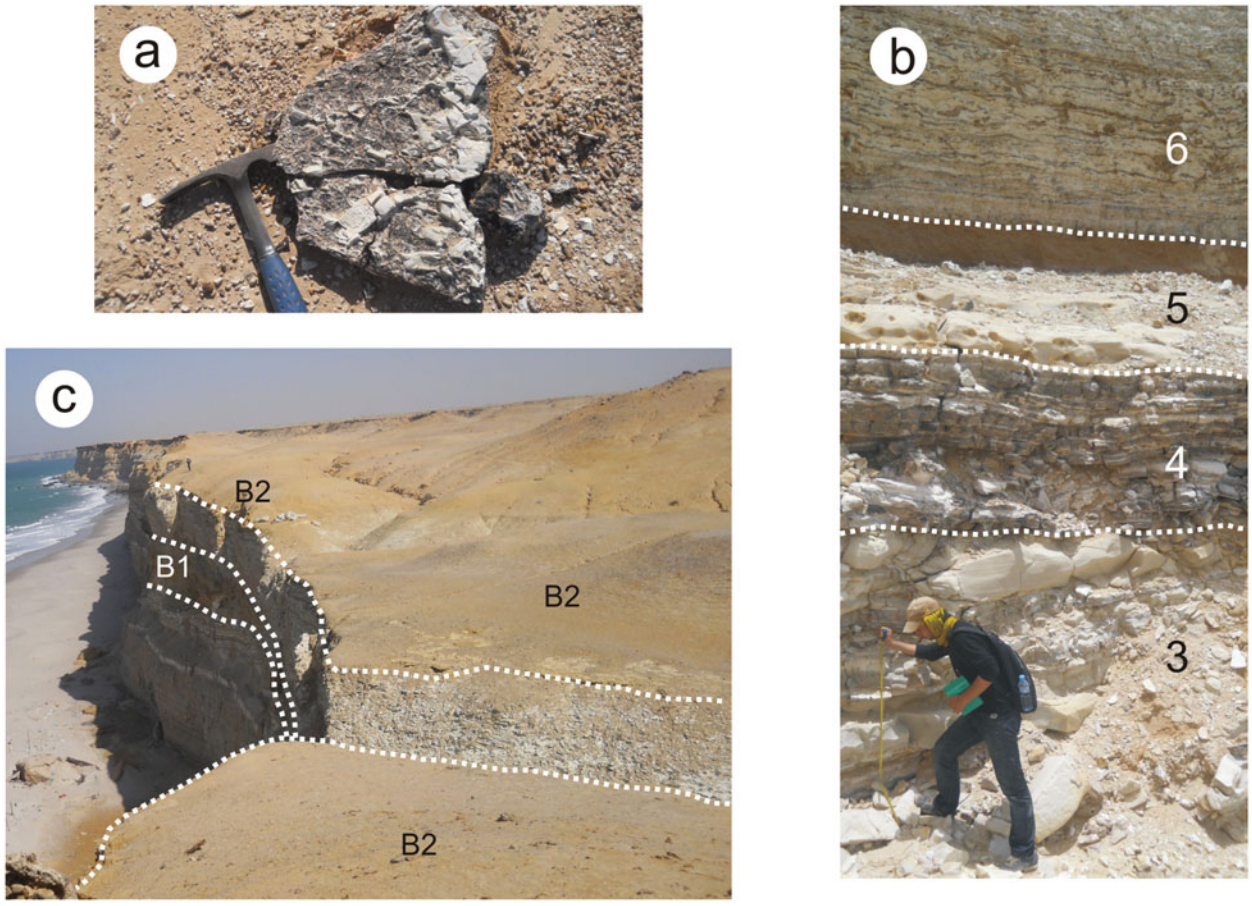


Figure 4. (Colour online) Field photographs showing: (a) an example of coprolite level; (b) a succession of grey limestone bar and beige sandy calcareous marl (lithofacies 3 in Fig. 2), black to brown or dark siliceous limestone with coprolites at its base (lithofacies 4), yellowish sandy marl rich in vertebrate fossil, fossil-bearing level B1 (lithofacies 5); and (c) a whitish marl with lenticular brown siliceous limestone (lithofacies 6).

(1967) remain hypothetical, and suffer from inconsistent observations. Ratschiller (1967, fig. 176) illustrated a beach cliff around Porto Rico, where he considered that the Aaiun Formation directly overlies the Lebtaina Formation, a formation underlying the Samlat Formation. However, it seems that what he considered as the Aaiun Formation actually corresponds to U3–5 of the Dakhla area, and that the Lebtaina Formation corresponds to U1–2. Although units U1 and U2 are attributed to the Guerran Member and units U3 and U4 to the Morcba Member, it is difficult to find the lithological subdivision described and proposed by Ratschiller (1967).

## 6. Palaeomagnetic analysis

Samples were analysed with the palaeomagnetic facilities housed at the iPHEP of the Université de Poitiers, France. Remanent magnetization was measured with a JR6 magnetometer combined with stepwise thermal or alternating field demagnetization in a magnetically shielded room. To better constrain the magnetic mineralogy, we studied the acquisition of isothermal remanent magnetization (IRM), and then the stepwise thermal demagnetization of three-axis differential IRM following the method of Lowrie (1990). The specimens were subjected to stepwise thermal demagnetization in steps up to 600 °C. The IRM was determined with a pulse electromagnet. Thermal demagnetization was conducted with a magnetic measurement thermal demagnetizer (MMTD80) shielded furnace. Progressive thermal demagnetization was carried out, in steps of 30–40 °C, from 100 °C until either the magnetization intensity fell below the noise level or the direction became erratic. The majority of specimens were submitted to stepwise alternating field (AF) demagnetization with increments of 5–10 mT, using a Molspin Ltd high-field shielded demagnetizer. Characteristic magnetization components were isolated by applying the method of Kirschvink (1980) to vector segments with a maximum angular deviation less than 15°.

### 6.a. Magnetic properties and characteristic directions

A set of rock magnetic experiments was conducted to characterize and identify the magnetic mineralogy of the main lithologies. We first analysed the acquisition of IRM up to 500 mT and its subsequent thermal demagnetization. Following the procedure described by

https://doi.org/10.1017/S0016756817000851 Published online by Cambridge University Press

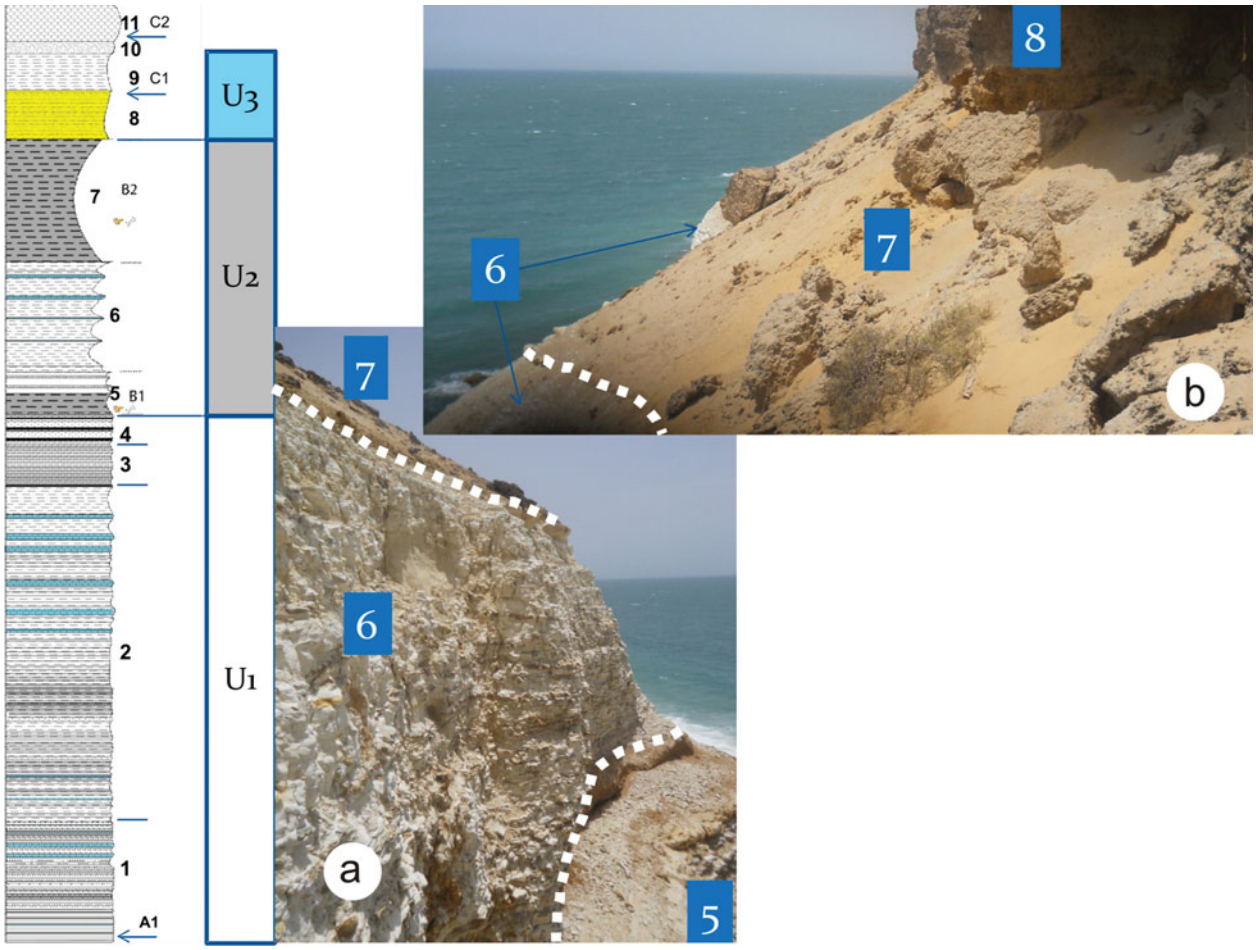


Figure 5. (Colour online) Garitas section: (a) lithofacies 6 forms the prominent ledge and (b) overlying muddy brown yellow sandstone corresponding to fossil-bearing level B2 (lithofacies 7).

Lowrie (1990), magnetic fields of 1, 0.4 and 0.12 T were successively applied to each of the three perpendicular directions prior to thermal demagnetization. The IRM acquisition curves (Fig. 10a) show a broad range of coercivities. The initial increase in magnetization up to 100–150 mT indicates the presence of low-coercivity minerals. Saturation was achieved between 300 and 500 mT, which indicates the presence of intermediate coercivity minerals.

Thermal demagnetization shows that the low-field (0.12 T) component is dominant; in Figure 10b and c the first drop appears on the soft and medium components between 300 °C and 350 °C, indicating the existence of magnetic mineral with soft coercivity, probably corresponding to low tititanomagnetite. The second drop is observed at 580 °C, indicating the presence of magnetite. The harder components, less than 25 % of the total IRM, decrease regularly up to temperatures of 300–350 °C and suggest the presence of a Fe-sulphide.

Thermomagnetic curves are routinely used in palaeomagnetism to identify remanence carriers. Low-field susceptibility measurements (*k–T* curves) were performed using a Bartington susceptibility meter (MS-2) equipped with furnace. Some specimens were heated up to 600 °C at a heating rate of 10 °C $min^{-1}$, and then cooled at the same rate (Fig. 10d). The thermomagnetic behaviour of bulk sediment samples shows very low magnetization, in agreement with the low intensity of the sample. Magnetization starts to increase at *c.* 400 °C, is maximal at *c.* 500 °C, and then decreases sharply to zero just before 600 °C. This is due to the presence of pyrite, a paramagnetic mineral that altered towards magnetite near 500 °C during the experiment (Strechie *et al*. 2002; Tudryn & Tucholka, 2004). Cooling curves indicate that magnetite is produced as a result of the thermal breakdown (Fig. 10d). No correct curve was obtained for the majority of samples because of the low initial signal of magnetic susceptibility.

The natural remanent magnetization displays moderately high values, starting at $8.8\times10^{-7}$ A $m^{-1}$ in siltstone levels and reaching up to *c.* $6.3\times10^{-4}$ A $m^{-1}$, with an average of $1.9\times10^{-4}$ A $m^{-1}$ (Fig. 11). After some step demagnetization, the magnetization intensity fell below noise level of the magnetometer (Fig. 12a) and the direction became erratic (Fig. 12b). Data resulting from AF and thermal demagnetization were plotted on orthogonal vector plots (Zijderveld, 1967). To determine characteristic magnetic directions, principal components analysis was carried out on all samples. These palaeomagnetic directions were then analysed using Fisher statistics to determine site

https://doi.org/10.1017/S0016756817000851 Published online by Cambridge University Press

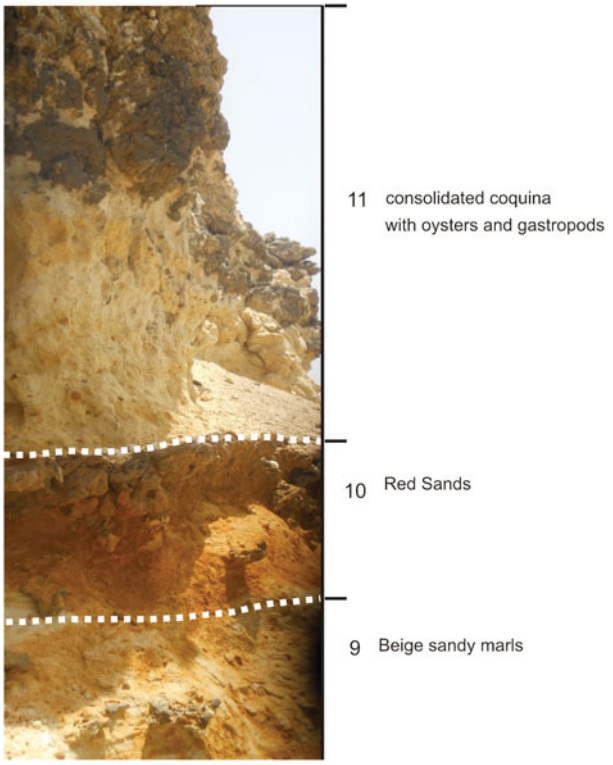


Figure 6. (Colour online) Field photographs showing the top of the Garitas section with lithofacies 9, 10 and 11.

mean declinations, mean inclinations and associated precision parameters.

Only tree strata at the upper part of the section give a coherent result of normal direction (Fig. 12c). The mean directions of ChRM are declination 324.4° and inclination 44.6° ($\alpha_{95}$ = 24.4, $\kappa$ = 6), and differ from the expected direction for this latitude (declination 352.2° and inclination 27.2°) (Fig. 12d).

## 7. Carbon isotope geochemistry results

Carbon isotopic values range from –27.8 ‰ (sample ARG15-2) to –22.1 ‰ (sample PTO15-11; Table 1). These data are in good agreement with the expected $\delta^{13}C$ values on organics at the Eocene–Oligocene interval (see Sarkar *et al*. 2003). Seven samples have total organic carbon (TOC) too low (<0.01 %) to perform reliable isotopic analysis.

In the Porto Rico section, the $\delta^{13}C_{org}$ curve shows the following successive values/trends from the base to the top (Fig. 13; Table 1): (1) relatively negative $\delta^{13}C_{org}$ value (–27.6 ‰) in the B1 fossil-bearing level, at the base of the section (lowermost part of unit U2); (2) relatively stable $\delta^{13}C_{org}$ values (from –25.1 to –24.3 ‰) in U2 (including the fossil-bearing B2 level); (3) relatively negative $\delta^{13}C_{org}$ value (*c.* –25.7 ‰) in the lower part of U3 (including the C1 fossil-bearing level); (4) relatively stable $\delta^{13}C_{org}$ values (from –25.2 to –24.6 ‰) in the upper part of U3; (5) prominent and rapid positive shift of $\delta^{13}C_{org}$ values from –26.2 ‰ to –22.1 ‰ in the uppermost part of U3 and U4; (6) negative shift of $\delta^{13}C_{org}$ values from –22.1 ‰ to –25.4 ‰ in the lower part of U5 (including the C2 fossil-bearing level); (7) positive shift of $\delta^{13}C_{org}$ values from –25.4 ‰ to –23.7 ‰ in the upper part of U5; and (8) negative shift of $\delta^{13}C_{org}$ values from –23.7 ‰ to –25.2 ‰ in the uppermost part of U5.

In the El Argoub section, the $\delta^{13}C_{org}$ curve shows the following successive values/trends from the base to the top (Fig. 13; Table 1): (1) prominent and rapid positive shift of $\delta^{13}C_{org}$ values from –27.8 ‰ to –23.4 ‰ in the uppermost part of U3 and U4; (2) negative shift of $\delta^{13}C_{org}$ values from –23.4 ‰ to –25.7 ‰ in the lower part of U5 (including the C2 fossil-bearing level); (3) positive shift of $\delta^{13}C_{org}$ values from –25.7 ‰ to –23.0 ‰ in the upper part of U5; and (4) negative shift of $\delta^{13}C_{org}$ values from –23.0 ‰ to –25.5 ‰ in the uppermost part of U5.

The $CaCO_3$ contents range over 0.0–76.9 % in the Porto Rico section and 0.0–45.3 % in the El Argoub section.

## 8. Discussion

The fossil content of the Dakhla deposits is rich and varied, mixing primarily selachians and marine mammals (cetaceans and sirenians). Ratschiller (1967) first mentioned the occurrence of fish teeth in the Eocene Guerran Member of the Samlat Formation. In the Dakhla area, a rich vertebrate fauna was discovered by Adnet, Cappetta & Tabuce (2010) in two levels: B1 and B2. The Eocene age proposed by Ratschiller (1967) and later by Adnet, Cappetta & Tabuce (2010) was based on palaeontological evidence. Indeed, the majority of selachian taxa (such as *Xiphodolamia serrata*, *Misrichthys stromeri* and *Cretolamna twiggsensis*) recovered in B1 and B2 are known elsewhere in deposits dating from the Bartonian and Priabonian ages (e.g. Qasr El Sagha Formation, Egypt; Qa'Faydat and the Wadi Esh-Shallala Formation, Jordan; or the Drazinda Shale Member of the Kirthar Formation, Pakistan; Adnet, Cappetta & Tabuce, 2010). Later, Zouhri *et al*. (2014) described five archaeocete cetacean species from level B1 and dugongid sirenians in level B2; faunal correlations with the late Eocene Epoch of Egypt indicate a Priabonian age for the B1 and B2 fossil assemblages.

Since 2013, our fieldwork allowed the discovery of new fossil-bearing levels in the stratigraphic sequence (A1, C1 and C2). The lowermost part of the Garitas section (U1; Figs 2, 3) has yielded a fossil-bearing level including a diverse assemblage of fish (e.g. *'Carcharias' koerti*, *Physogaleus* aff. *tertius*, *Coupatezia* spp., *Merabatis* sp., *Burhnamia* sp., *Cyladrincanthus* sp.). In the Porto Rico section (Fig. 7), two stratigraphically distinct levels have yielded fossil vertebrates. Level C1, located at the base of U3, has yielded an assemblage of selachians (e.g. *Carcharhinus* spp., *Carcharias* sp., *Pristis* cf. *lathami*, *Pastinachus* sp., *Aetobatis* cf. *irregularis*). Above in the section, the base of U4 has yielded a fossil assemblage

https://doi.org/10.1017/S0016756817000851 Published online by Cambridge University Press

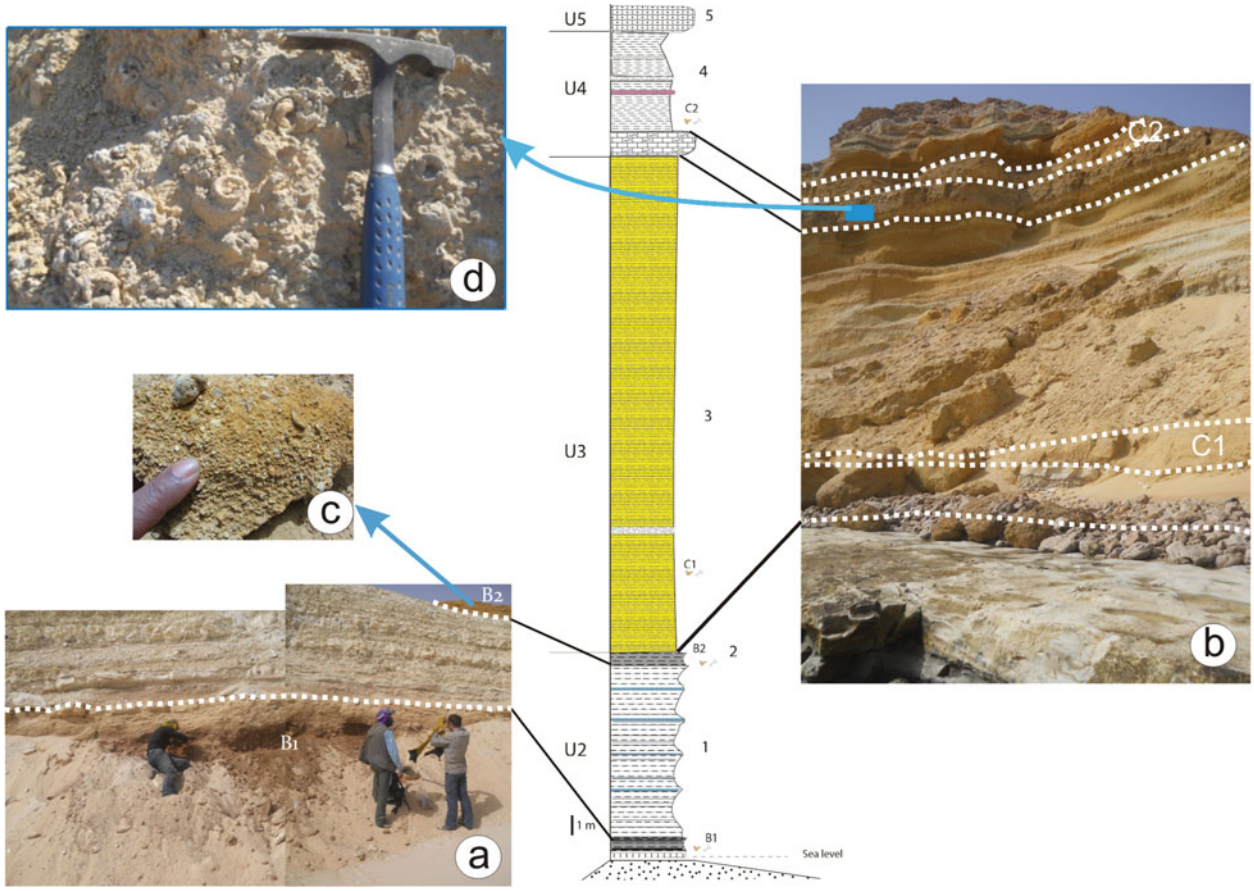


Figure 7. (Colour online) Porto Rico section: (a) general view of the lower part of the section with the fossil-bearing levels B1 and B2; (b) exposure of Unit U3 corresponding to lithofacies 3, which consists of a thick multicolour sandy marl series interstratified by sandstone with limestone concretions (we can see the position of fossil-bearing levels C1 and C2); (c) photograph showing the abundant selachian teeth of the B2 level; and (d) landmark level of gastropod and oyster coquina.

(C2) of marine and estuarine invertebrates (lamellibranches) and vertebrates (including fishes, turtles, crocodiles and selachians resembling C1), together with terrestrial mammals (including rodents, primates, hyracoids, an elephant shrew and creodonts). A strictly similar fossil assemblage was found in the El Argoub section in equivalent deposits (i.e. at the base of U4).

The mammal fossils of C2 (Porto Rico and El Argoub) consist of isolated teeth, but also partial jaws and bone fragments. Among the mammals, afrotherians are illustrated by a herodotiine macroscelid (*Herodotius* aff. *pattersoni*) and several 'saghatheriid' hyracoids, among which is a species of *Saghatherium*. Primates include an oligopithecid anthropoid (*Catopithecus* aff. *browni*) and an indeterminate afrotarsiid. Rodents are much more abundant and represented by members of two phylogenetically distinct groups: Hystricognathi and Anomaluroidea. Several tens of isolated teeth of anomaluroids indicate the presence of two distinct families, Anomaluridae and Nonanomaluridae, and possibly the ancestral family Zegdoumyidae, represented by five new species (*Argouburus minutus*, *Paranomalurus riodeoroensis*, *Dakhlamys ultimus*, *Oromys zenkerellinopsis* and *Nonanomalurus parvus*; see Marivaux *et al.* 2017*a* ). Regarding hystricognaths Marivaux *et al.* (2017*b*), distinct taxa are recognized including several 'phiomyid'-like representatives (*Birkamys* aff. *korai*, *Mubhammys* sp. nov., ?*Phiocricetomys* sp., *Neophiomys* sp. nov. and a new genus and species) and gaudeamurids (*Gaudeamus* cf. *hylaeus* and *G.* cf. *aslius*). Most of these Dakhla C2 mammals (with the exception of anomaluroids; Marivaux *et al.* 2017*a* ), or at least their close relatives, have originally been described from well-known Egyptian localities of the Jebel Qatrani Formation (Fayum Depression) dating from the latest Eocene (L-41; Hyracoidea: Rasmussen & Gutiérrez, 2010; Macroscelididae: Simons, Holroyd & Bown, 1991; Primates: Simons 1995; Simons & Rasmussen 1996; Seiffert, 2012; Rodentia: Sallam, Seiffert & Simons, 2011; Sallam & Seiffert, 2016) or the early Oligocene (Hyracoidea: Rasmussen & Gutiérrez, 2010; Rodentia: Wood, 1968). This faunal similarity therefore indicates a latest Eocene – early Oligocene timeframe for the fossiliferous concentration of level C2 of the Pto-Arg sector.

Here we performed new chemostratigraphic investigation using carbon isotopes from dispersed organic matter ($\delta^{13}C_{org}$) on the Porto Rico and El Argoub

https://doi.org/10.1017/S0016756817000851 Published online by Cambridge University Press

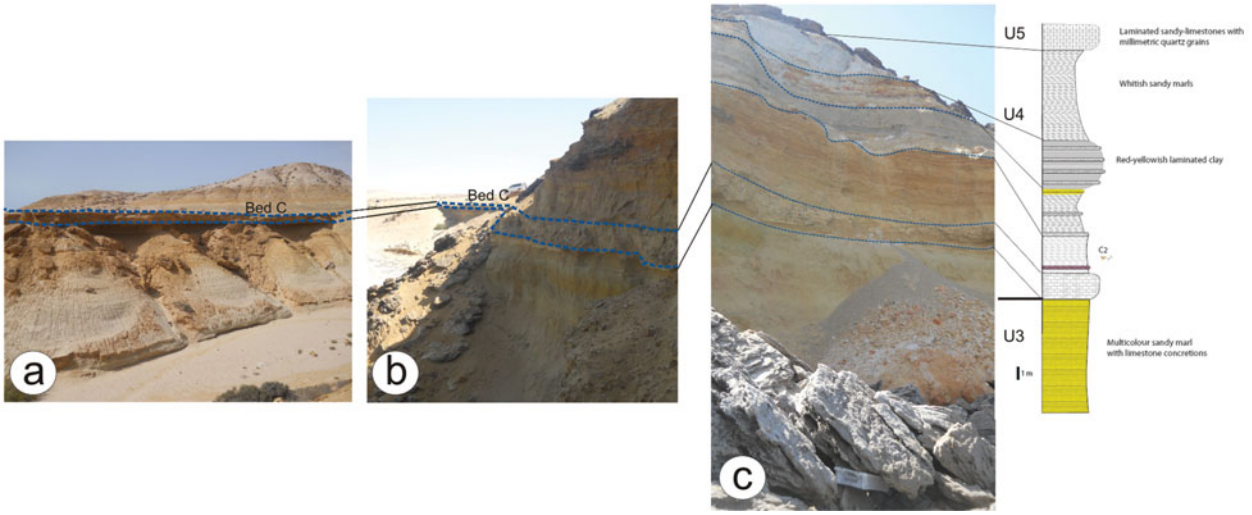


Figure 8. (Colour online) Field photographs and measured section of north Porto Rico and El Argoub areas: (a) section located 2 km north of El Argoub village; and (b, c) sections *c.* 6 km north of Porto Rico. See the landmark level consisting of gastropod and oyster coquina at the lower part of U4.

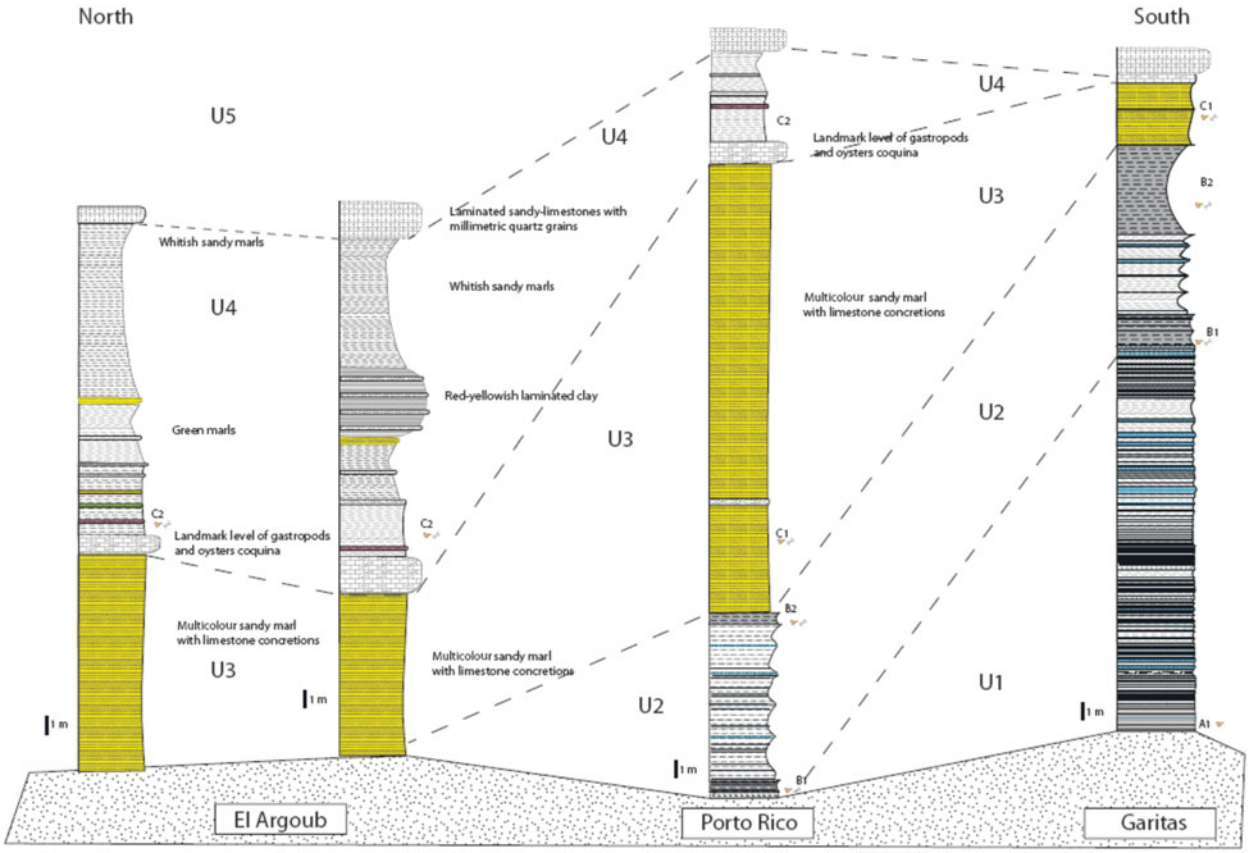


Figure 9. (Colour online) Outline correlation between cross-sections from Garitas to El Argoub.

sections in order to refine the stratigraphic framework of the Samlat Formation in the Dakhla area. As mentioned above, Adnet, Cappetta & Tabuce (2010) suggested a Bartonian–Priabonian age for the fossil-bearing levels B1 and B2 on the basis of the selachian fauna. Later, Zouhri *et al*. (2014) refined the age of level B1 and proposed one of early–middle Priabonian on the basis of the cetacean fauna. These authors also suggested a Priabonian age for level B2 on the basis of the sirenian fauna. This implies that the lower part of the studied sections containing levels B1 and B2 is (early–middle) Priabonian in age, thereby suggesting that the upper part of the section is Priabonian in age or younger.

The Eocene–Oligocene boundary (EOB; *c.* 34 Ma) is the largest global cooling of the Cenozoic Era and

https://doi.org/10.1017/S0016756817000851 Published online by Cambridge University Press

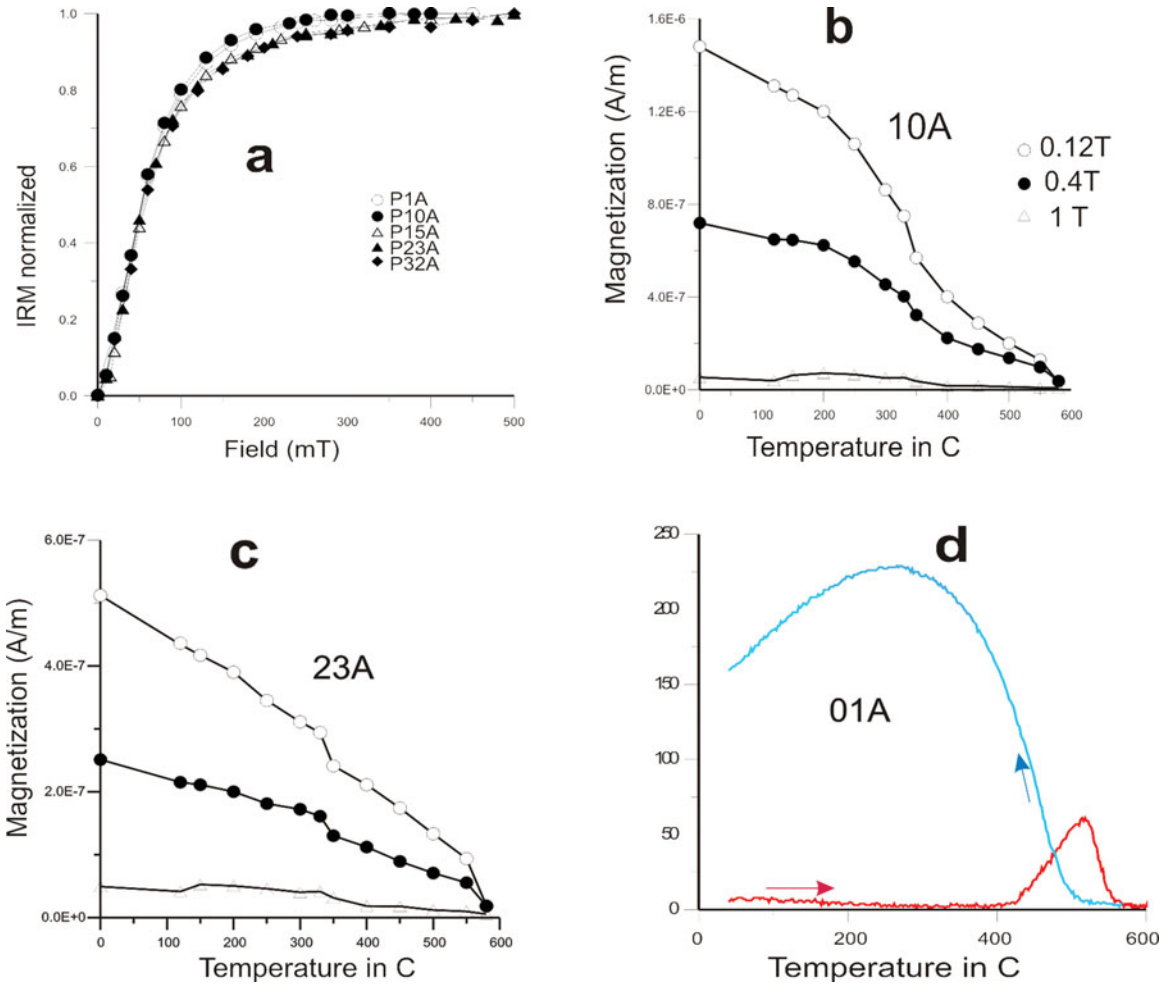


Figure 10. (Colour online) Palaeomagnetic analysis: (a) acquisition of isothermal remanent magnetization (IRM) (normalized values) curves of same samples, with most of the magnetization acquired below 200 mT and saturation achieved at 300 mT; (b, c) stepwise thermal demagnetization of the IRM components; and (d) thermomagnetic curve of sample, where magnetic iron sulphides where suspected to be present in the samples.

led the Earth's climatic system changing from a greenhouse to an icehouse mode; this change is well documented in the marine setting (e.g. Bohaty, Zachos & Delaney, 2012) and, to a lesser extent, in the continental setting (e.g. Tramoy *et al*. 2016). Initiated during late Eocene time, the cooling interval comprises several isotopic events which have been coded by Miller, Wright & Fairbanks (1991). The oldest of the events, coded Oi-1, the Eocene–Oligocene (climate) transition or EOT, is associated with major $\delta^{18}O$ and $\delta^{13}C$ positive shifts which started during late Eocene time and ended during early Oligocene time (e.g. Coxall *et al.* 2005; Katz *et al*. 2008; Lear *et al*. 2008). Using a high-resolution carbon isotope study of the Ocean Drilling Program (ODP) site 1218, Erhardt, Pälike & Paytan (2013) showed that the carbon and oxygen positive shifts of the Oi-1 event are followed by two positive $\delta^{13}C$ and $\delta^{18}O$ excursions called Oi-1a and Oi-1b, of early Oligocene age. This isotopic pattern was also observed by Zhifei *et al*. (2004) in ODP Leg 208 Site 1262, 1265 and 522.

In the Porto Rico (Pto) and El Argoub (Arg) sections (this study; Fig. 13), the Oi-1 event initiates in the uppermost part of the U3 lithological unit (*c.* 2 m below the C2 level) and ends below the C2 level. This isotopic event is followed by one positive excursion (positive shift followed by a negative shift), interpreted here as Oi-1a. In summary, the C2 level is clearly above the Oi-1; as such, it is probably earliest Oligocene in age.

Lower, the B1 and B2 fossil-bearing levels are dated as Priabonian in age by the selachian, cetacean and sirenian faunas (see above). The C1 level is located in a negative $\delta^{13}C$ excursion (Fig. 13). This latter should correspond to the carbon isotope excursion observed in the Priabonian strata (NP19-20 Zones). The B1 level shows a negative $\delta^{13}C$ value, most probably corresponding to the negative $\delta^{13}C$ values in the lower Priabonian NP18 Zone (Fig. 13).

The palaeomagnetic analysis show that the only normal polarity is represented by tree strata situated 2 m above the C1 fossiliferous level. Although the rock magnetic properties suggest that the natural remanent magnetization (NRM) may be of primary origin, we evaluate other criteria to infer the origin of the observed characteristic remanence. The *in situ* site mean directions differ significantly from the

https://doi.org/10.1017/S0016756817000851 Published online by Cambridge University Press

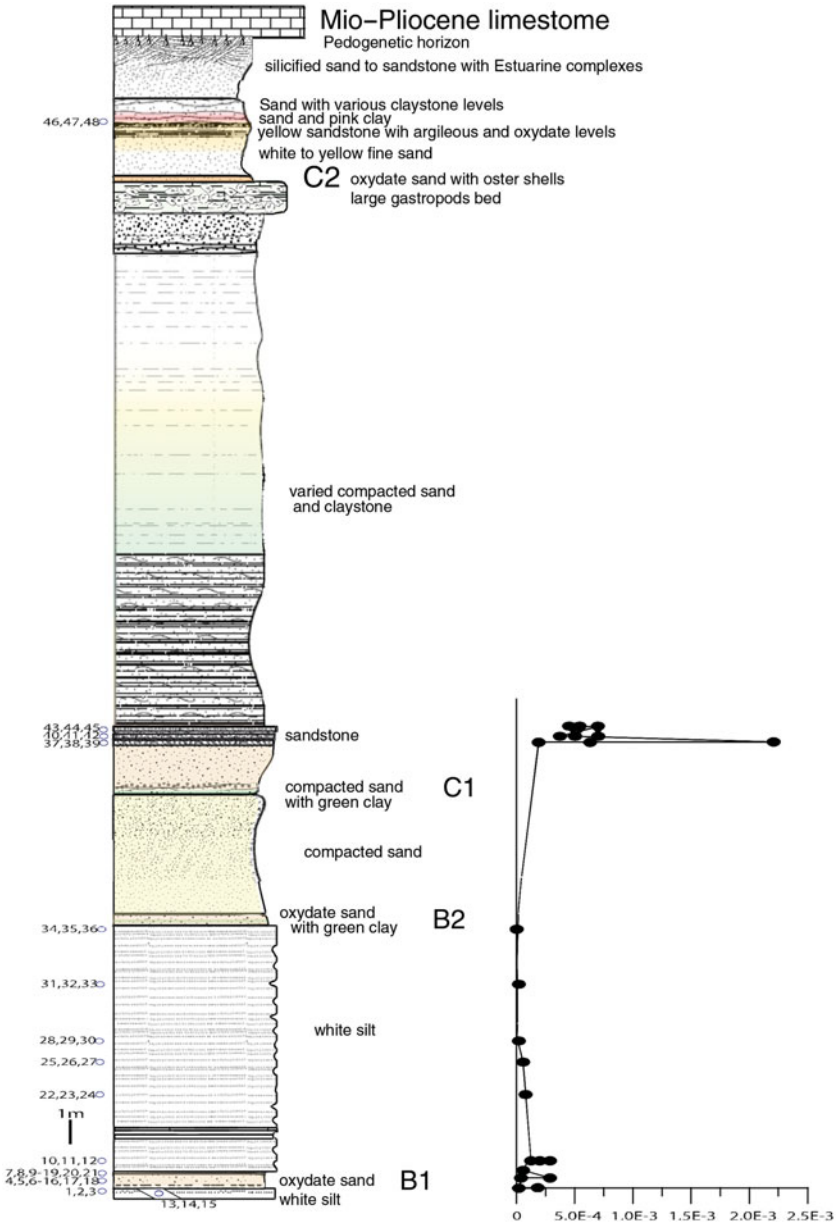


Figure 11. (Colour online) Porto Rico section and position of palaeomagnetic sampling, and the NRM intensities plotted against lithostratigraphic position (right curve). Note the position of the fossil-bearing levels B1, B2, C1 and C2.

direction of the axial geocentric dipole at the latitude of the site (Fig. 12d) and therefore exclude a recent magnetic overprint. Correlation of the Porto Rico section with the geomagnetic polarity timescale (GPTS) of Gradstein *et al*. (2012) was performed by considering the earliest Oligocene age discussed above for C2 level and the Priabonian age for B2 and C1. Taking into account the biochronological age, the normal polarity might then be correlated to Chron C16n.

Our new chemostratigraphic and palaeomagnetic data suggest that the C2 fossil-bearing level of Dakhla is clearly located above the Oi-1 event and below the Oi-1a event. The Oi-1 event, bringing the major cooling, is recognized by many authors to have occurred a few 100 ka later than the Global Boundary Stratotype Section and Point (GSSP) of the Rupelian Age (Eocene–Oligocene boundary; Vandenberghe, Hilgen & Speijer, 2012). The GSSP of the Eocene–Oligocene boundary is defined in the Massignano section (Italy), and the key marker of the GSSP is the extinction of the hantkeninid planktonic foraminifera which lies within nannofossil Zone NP21 (Premoli-Silva & Jenkins, 1993). Katz *et al*. (2008) showed that: (1) the Oi-1 event is located around the transition of Chron C13r and C13n (33.545 Ma); and (2) the Oi-1a event is located around the transition of Chron C13n and C12r. This suggests that the C2 level, located just above the Oi-1 event and below the Oi-1a event, is a few 100 ka above the Eocene–Oligocene boundary within the nannofossil Zone NP21 and into the magnetic polarity Chron 13n. Interestingly, as mentioned above, Gingerich (1993) suggested that the L-41 level

https://doi.org/10.1017/S0016756817000851 Published online by Cambridge University Press

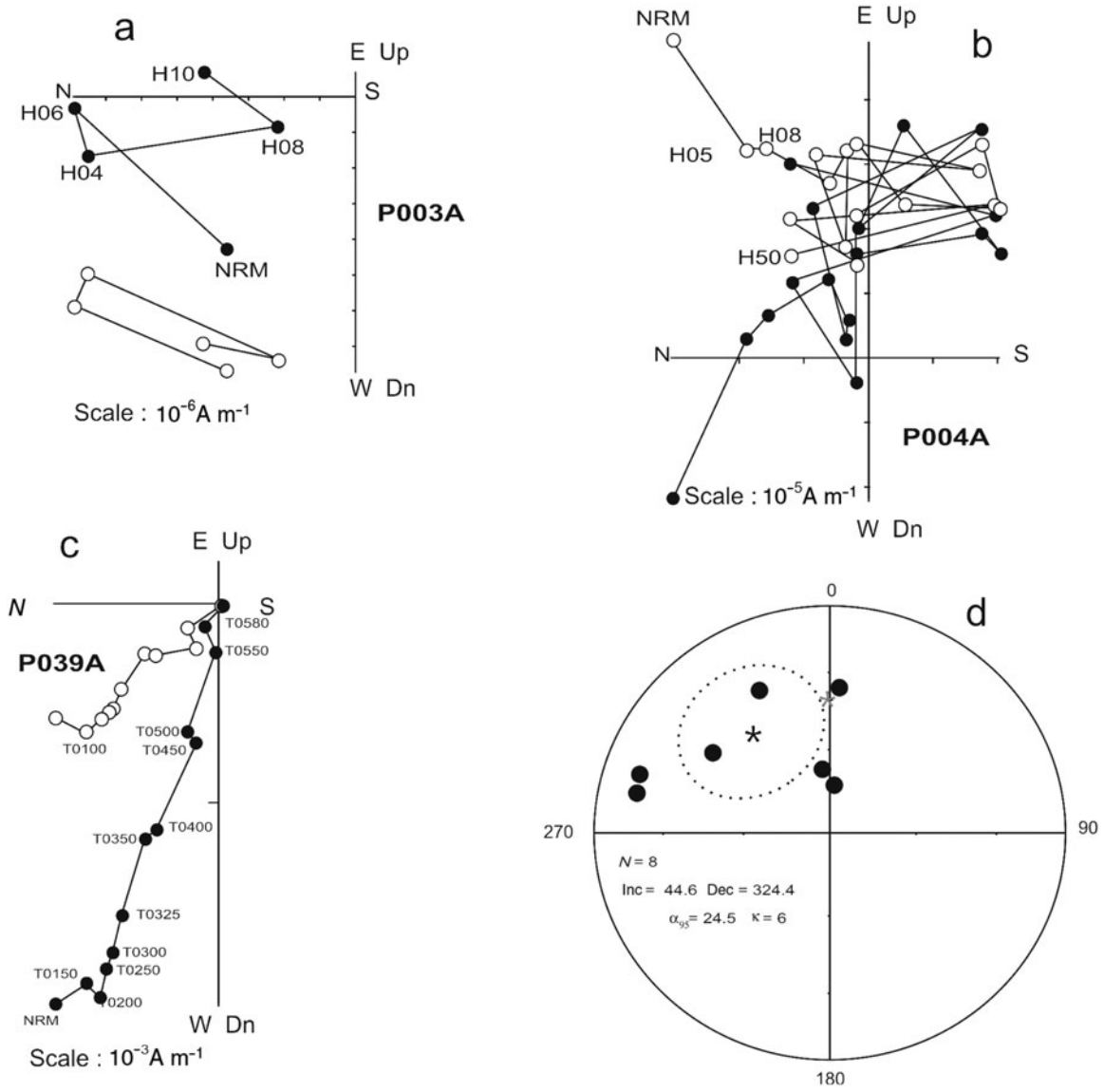


Figure 12. Demagnetization plots of the samples. The solid (open) symbols represent horizontal (vertical) projections: (a) at 10 mT, the magnetization intensity falls below the noise level of the magnetometer; (b) example of samples with erratic direction; (c) example of samples with normal polarity from the site situated 2 m above the C1 fossil-bearing level; and (d) equal-area projection and Fisher statistics of the reliable characteristic remanent magnetization (ChRM) direction. The 95 % confidence ellipse for the normal (solid star) mean directions is indicated (inclination 44.6°, declination 324.4°). The asterisk represents the geocentric axial dipole of the Porto Rico latitude.

(lower part of the Jbel Qatrani Formation) is located in the lower Oligocene strata. Underwood, King & Steurbaut (2013) place the base of the Jebel Qatrani Formation close to the base of Chron C13n. On the other hand, Seiffert (2006) concluded that the L-41 of Fayum bed falls within a zone of reverse polarity and is correlated with Chron 13r, of late Eocene age, that is, older than the C2 level of Dakhla. The new rodent assemblage from the lowest Oligocene strata of Dakhla (Sahara, Morocco) therefore represents the first Oligocene record of rodents from northwestern Saharan Africa, especially from the Atlantic margin of that landmass. The carbon isotope chemostratigraphy confirms that the lower part of the studied sections containing levels B1 and B2 is early–middle Priabonian in age.

Our knowledge of the mammal faunas documenting the early Oligocene Epoch of Afro-Arabia has so far derived from contemporary localities found in northern Egypt (Fayum Depression), Libya (Zallah Oasis) and Oman (Dhofar Province) (Fejfar, 1987; Sallam, Seiffert & Simons, 2011; Coster *et al.* 2010, 2012; Sallam & Seiffert, 2016). This new earliest Oligocene mammal fauna from the northern Atlantic margin of Africa is of great interest because it documents for the first time the diversity of micromammals, especially rodents. Biochronology and C isotope chemostratigraphy provide an Oligocene age constraint of C2 fossiliferous level, and therefore increase our understanding of the timing of mammal evolution and environmental change in North Africa at that time.

https://doi.org/10.1017/S0016756817000851 Published online by Cambridge University Press

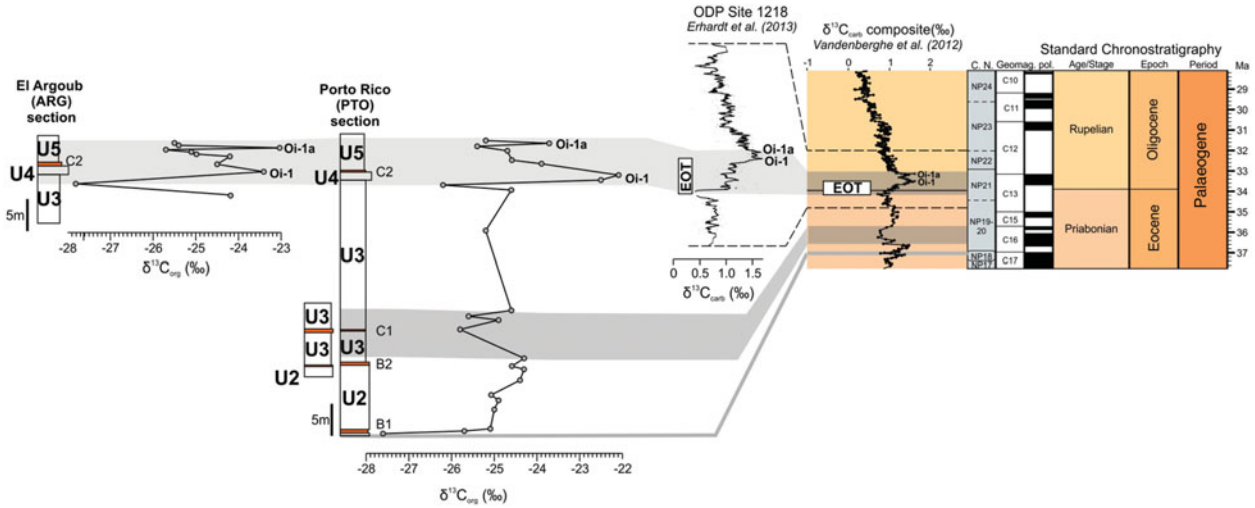


Figure 13. (Colour online) Carbon isotope values (‰ VPDB) of the Porto Rico and El Argoub sections, compared to $\delta^{13}C$ curves around the Eocene–Oligocene transition at ODP Site 1218 (Erhardt, Pälike & Paytan, 2013) and reference $\delta^{13}C$ composite curve (Cramer *et al.* 2009; modified by Vandenberghe, Hilgen & Speijer, 2012). EOT – Eocene–Oligocene Transition; U1–U5 – lithological units defined in the text; B1, B2, C1, C2 – fossil-bearing levels.

**Acknowledgements.** We would like to thank Abdallah Tarmidi and Mbarek Fouadasi for their help during the fieldwork. Financial support during the fieldwork was provided by the French ANR EVAH (ANR-09-BLAN-0238) and ANR-ERC PALASIAFRICA (ANR-08-JCJC-0017) programs, the ISE-M UMR 5554 CNRS/UM/IRD/EPHE, CNRS-CoopIntEER171834 and iPHEP UMR CNRS 7262. CN and JY thank the Belgian Science Policy Office, project BR/121/A3/PALEURAFRICA. We also thank E. R. Seiffert (University of Southern California, Los Angeles, USA) and another anonymous reviewer, who provided formal reviews of this manuscript that enhanced the final version.

## References

Adnet, S., Cappetta, H. & Tabuce, R. 2010. A Middle–Late Eocene vertebrate fauna (marine fish and mammals) from southwestern Morocco; preliminary report: age and palaeobiogeographical implications. *Geological Magazine* **147**, 860–70.

Benammi, M., Elkati, I., Adnet, S., Marivaux, L., Tabuce, R., Surault, J., Baidder, L., Saddiqi, O. & Benammi, M. 2014a. Corrélation de coupes lithostratigraphiques le long des falaises côtières dans la region d'El Argoub (Dakhla, Maroc). *In Proceedings of Second North African Vertebrate Palaeontology Congress-NAVEP2*, Ouarzazate, Morocco, 1–8 September, Abstracts, p. 37.

Benammi, M., Elkati, I., Adnet, S., Marivaux, L., Tabuce, R., Surault, J., Baidder, L., Saddiqi, O. & Benammi, M. 2014b. Preliminary paleomagnetic data in the Dakhla, Southwestern Moroccan Sahara. In *Proceedings of Second North African Vertebrate Palaeontology Congress-NAVEP2*, Ouarzazate, Morocco, 1–8 September, Abstracts, p. 40.

Bohaty, S. M., Zachos, J. C. & Delaney, M. L. 2012. Foraminiferal Mg/Ca evidence for Southern Ocean cooling across the Eocene/Oligocene transition. *Earth and Planetary Science Letters* **317–8**, 251–61.

Coster, P., Benammi, M., Lazzari, V., Billet, G., Martin, T., Salem, M., Abolhassan Bilal, A., Chaimanee, Y., Schuster, M., Valentin, X., Brunet, M. & Jaeger, J.-J. 2010. *Gaudeamus lavocati* sp. nov. (Rodentia, Hystricognathi) from the lower Oligocene of Zallah, Libya: first African Caviomorph? *Naturwissenschaften* **97**, 697–70.

Coster, P., Benammi, M., Salem, M., Bilal Awad, A., Chaimanee, Y., Valentin, X., Brunet, M. & Jaeger, J. J. 2012. New hystricognathous rodent from the Early Oligocene of central Libya, (Zallah Oasis, Sahara Desert): systematic, phylogenetic, and biochronologic implications. *Annals of Carnegie Museum* **80**, 239–59.

Coxall, H. K., Wilson, P. A., Pälike, H., Lear, C. H. & Backman, J. 2005. Rapid stepwise onset of Antarctic glaciation and deeper calcite compensation in the Pacific Ocean. *Nature* **433**, 53–7.

Cramer, B. S., Toggweiler, J. R., Wright, J. D., Katz, M. E. & Miller, K. G. 2009. Ocean overturning since the Late Cretaceous: inferences from a new benthic foraminiferal isotope compilation. *Paleoceanography* **4**(24), doi: 10.1029/2008PA001683.

Davison, I. 2005. Central Atlantic margin basins of North West Africa: geology and hydrocarbon potential (Morocco to Guinea). *Journal of African Earth Sciences* **43**(1–3), 254–74.

Davison, I. & Dailly, P. 2010. Salt tectonics in the Cap Boujdour Area, Aaiun Basin, NW Africa. *Marine and Petroleum Geology* **27**, 435–41.

Deperet, C. 1912. Sur l'âge des couches du Rio de Oro. *Comptes Rendus de l'Académie des Sciences* **13**, 123–4.

Erhardt, A. M., Pälike, H. & Paytan, A. 2013. High-resolution record of export production in the eastern equatorial Pacific across the Eocene-Oligocene transition and relationships to global climatic records. *Paleoceanography* **28**, 130–42.

Fejfar, O. 1987. Oligocene rodents from Zallah Oasis, Libya. *Münchner Geowissenschaftliche Abhandlungen* **A10**, 265–8.

Front, Y. & Sague, N. 1911. Les formations géologiques du Rio de Oro, Sahara espagnol. *Bulletin de la Société Géologique de France* **4**, 212–7.

Gingerich, P. H. 1993. Oligocene age of the Gebel Qatrani Formation, Fayum, Egypt. *Journal of Human Evolution* **24**, 207–18.

https://doi.org/10.1017/S0016756817000851 Published online by Cambridge University Press

Gradstein, F. M., Ogg, J. G., Schmitz, M. D. & Ogg, G. M. (eds) 2012. *The Geologic Time Scale 2012*. Amsterdam, Netherlands: Elsevier, 1144 pp.

Joleaud, L. 1907. Note sur quelques dents de Poissons fossiles du Rio de Oro (Sahara occidental). *Bulletin de la Société Géologique de France* **7**, 514.

Katz, M. E., Miller, K. G., Wright, J. D., Wade, B. S., Browning, J. V., Cramer, B. S. & Rosenthal, Y. 2008. Stepwise transition from the Eocene greenhouse to the Oligocene icehouse. *Nature Geosciences* **1**, 329–34.

Kirschvink, J. L. 1980. The least-square line and plane and analysis of palaeomagnetic data. *Geophysical Journal of the Royal Astronomical Society* **62**, 699–718.

Klingelhoefer, F., Labails, C., Cosquer, E., Rouzo, S., Géli, L., Aslanian, D., Olivet, J.-L., Sahabi, M., Nouzé, H. & Unternehr, P. 2009. Crustal structure of the SW-Moroccan margin from wide-angle and reflection seismic data (the Dakhla experiment) Part A: Wide-angle seismic models. *Tectonophysics* **468**, 63–82.

Kolonic, S., Sinninghedamsté, J. S., Böttcher, M. E., Kuypers, M. M. M., Kuhnt, W., Beckmann, B., Scheeder, G. & Wagner, T. 2002. Geochemical characterization of Cenomanian/Turonian black shales from the Tarfaya Basin (SW Morocco). *Journal of Petroleum Geology* **25**, 325–50.

Lear, C. H., Bailey, T. R., Pearson, P. N., Coxall, H. K. & Rosenthal, Y. 2008. Cooling and ice growth across the Eocene-Oligocene transition. *Geology* **36**, 251–4.

Lecointre, G. 1962. Sur la géologie de la presqu'ile de villa Cisneron, Rio de Oro. *Comptes Rendus de l'Académie des Sciences* **254**, 1121–2.

Lecointre, G. 1966. Néogène et Quaternaire du Rio de Oro (Maroc Espagnol). *Comptes Rendus de l'Académie des Sciences* **10**, 404–5.

Lowrie, W. 1990. Identification of ferrimagnetic minerals in rock by coercivity and unblocking temperature properties. *Geophysical Research Letters* **17**, 159–62.

Marivaux, L., Adnet, S., Benammi, M., Tabuce, R. & Benammi, M. 2017a. Anomaluroid rodents from the earliest Oligocene of Dakhla, Morocco, reveal the long-lived and morphologically conservative pattern of the Anomaluridae and Nonanomaluridae during the Tertiary in Africa. *Journal of Systematic Palaeontology* **15**(7), 539–69.

Marivaux, L., Adnet, S., Benammi, M., Tabuce, R., Yans, Y. & Benammi, M. 2017b. Earliest Oligocene hystricognathous rodents from the Atlantic margin of Northwestern Saharan Africa (Dakhla, Morocco): systematic, paleobiogeographical and paleoenvironmental implications. *Journal of Vertebrate Paleontology*, published online September 2017, doi: 10.1080/02724634.2017.1357567.

Miller, K. G., Wright, J. D. & Fairbanks, R. G. 1991. Unlocking the ice house: Oligocene-Miocene oxygen isotopes, eustasy and margin erosion. *Journal of Geophysical Research* **96**, 6829–48.

Ortlieb, L. 1975. Recherches sur les formations plio-quaternaire du littoral Ouest Saharien (28° 30′-20° 40′). PhD thesis, Pierre et Marie-Curie University, Paris VI. Published thesis (Travaux et Documents de l'ORSTOM, **48**, 267 pp).

Premoli-Silva, I. & Jenkins, D. G. 1993. Decision on the Eocene-Oligocene boundary stratotype. *Episodes* **16**, 379–82.

Ranke, U., Von Raad, U. & Wissmann, G. 1982. Stratigraphy, facies, and tectonic development of on- and offshore Aaiun-Tarfaya Basin: a review. In *Geology of the North West African Continental Margin* (ed. U. Von Raad), pp. 86–104. Berlin: Springer-Verlag.

Rasmussen, D. T. & Gutiérrez, M. 2010. Hyracoidea. In *The Cenozoic Mammals of Africa* (eds L. Werdlin & W. J. Sanders), pp. 123–46. Berkeley: University of California Press.

Ratschiller, L. K. 1967. Sahara, correlazioni geologico-litostratigrapfiche fra Sahara Centrale ed Occidentale. *Memoire del Museo Tridentino di Scienze Naturali* **16**, 55–190.

Rjimati, E., Zemmouri, A., Benlakhdim, A., Amzaehou, M., Essalmani, B., Mustaphi, H., Haimouk, M. & Hamidi, F. 2008. Carte Géologique du Maroc. Ad-Dakhla, 1/100 000. *Notes et Mémoires Service Géologique du Maroc*, 487.

Sachse, V. F., Heim, S., Jabour, H., Kluth, O., Schümann, T., Aquit, M. & Littke, R. 2014. Organic geochemical characterization of Santonian to Early Campanian organic matter-rich marls (Sondage No. 1 cores) as related to OAE3 from the Tarfaya Basin, Morocco. *Marine and Petroleum Geology* **56**, 290–304.

Sachse, V. F., Littke, R., Heim, S., Kluth, O., Schober, J., Boutib, L., Jabour, H., Perssen, F. & Sindern, S. 2011. Petroleum source rocks of the Tarfaya Basin and adjacent areas, Morocco. *Organic Geochemistry* **42**, 209–27.

Saddiqi, O., Rjimati, E., Michard, A., Soulaimani, A. & Ouanaimi, H. 2015. Recommended Geoheritage Trails in Southern Morocco: A 3 Ga Record Between the Sahara Desert and the Atlantic Ocean. In *From Geoheritage to Geoparks, Case Studies from Africa and Beyond* (eds E. Errami, B. Margaret & S. Vic), pp. 91–108. Switzerland: Springer.

Sallam, H. M. & Seiffert, E. R. 2016. New phiomorph rodents from the latest Eocene of Egypt, and the impact of Bayesian "clock" based phylogenetic methods on estimates of basal hystricognath relationships and biochronology. *PeerJ* **4**, e1717.

Sallam, H. M., Seiffert, E. R. & Simons, E. L. 2011. Craniodental morphology and systematics of a new family of hystricognathous rodents (Gaudeamuridae) from the Late Eocene and Early Oligocene of Egypt. *PLoS ONE* **6**, e16525eol.

Sarkar, A., Sarangib, S., Ebiharac, M., Bhattacharyad, S. K. & Raye, A. K. 2003.Carbonate geochemistry across the Eocene/Oligocene boundary of Kutch, western India: implications to oceanic O2-poor condition and foraminiferal extinction. *Chemical Geology* **201**, 281–93.

Seiffert, E. R. 2006. Revised age estimates for the later Paleogene mammal faunas of Egypt and Oman. *Proceedings of the National Academy of Sciences of the USA* **103**, 5000–5.

Seiffert, E. R. 2012. Early primate evolution in Afro-Arabia. *Evolutionary Anthropology* **21**, 239–53.

Simons, E. L., Holroyd, P. A. & Bown, T. M. 1991. Early Tertiary elephant shrews from Egypt and the origin of the Macroscelidea. *Proceedings of the National Academy of Sciences of the USA* **88**, 9734–7.

Simons, E. L. & Rasmussen, D. T. 1996. Skull of *Catopithecus browni*, an early Tertiary catarrhine. *American Journal of Physical Anthropology* **100**, 261–92.

Storme, J.-Y., Devleeschouwer, X., Schnyder, J., Cambier, G., Baceta, J. I., Pujalte, V., Iacumin, P. & Yans, J. 2012. Paleocene/Eocene boundary section at Zumaia (Basque-Catabric Basin) revisited: new insights from high resolution magnetic susceptibility and carbon

https://doi.org/10.1017/S0016756817000851 Published online by Cambridge University Press

isotope chemostratigraphy on organic matter ($\delta^{13}C_{org}$). *Terra Nova* **24**, 310–7.

Strechie, C., Andre, F., Jelinowska, A., Tucholka, P., Guichard, F., Lericolais, G. & Panin, N. 2002. Magnetic minerals as indicators of major environmental change in Holocene Black Sea sediments: preliminary results. *Physics Chemistry Earth* **27**, 1363–70.

Tramoy, R., Salpin, M., Schnyder, J., Person, A., Sebilo, M., Yans, J., Vaury, V., Fozzani, J. & Bauer, H. 2016. Stepwise paleoclimate change across the Eocene-Oligocene transition recorded in continental NW Europe by mineralogical assemblages and $\delta^{15}N_{org}$ (Rennes Basin, France). *Terra Nova* **28**, 212–20.

Tudryn, A. & Tucholka, P. 2004. Magnetic monitoring of thermal alteration for natural pyrite and greigite. *Acta Geophysica Polonica* **52**, 509–20.

Underwood, C. J., King, C. & Steurbaut, E. 2013. Eocene initiation of Nile drainage due to East African uplift. *Palaeogeography, Palaeoclimatology, Palaeoecology* **392**, 138–45.

Vandenberghe, N., Hilgen, F. J. & Speijer, R. 2012. The Paleogene Period. In *The Geological Time Scale* (eds F. M. Gradstein, J. G. Ogg, M. D. Schmitz & G. M. Ogg), pp. 855–921. Oxford: Elsevier Science Ltd.

Wood, A. E. 1968. Part II: The African Oligocene Rodentia. In *Early Cenozoic Mammalian Faunas Fayum Province, Egypt* (ed. J.E. Remington), pp. 23–105. New Haven, Connecticut: Peabody Museum of Natural History, Yale University.

Yans, J., Gerards, T., Gerrienne, P., Spagna, P., Dejax, J., Schnyder, J., Storme, J.-Y. & Keppens, E. 2010. Carbon-isotope of fossil wood and dispersed organic matter from the terrestrial Wealden facies of Hautrage (Mons basin, Belgium). *Palaeogeography, Palaeoclimatology, Palaeoecology* **291**, 85–105.

Zhifei, L., Shouting, T., Quanhong, Z., Xinrong, C. & Wei, H. 2004. Deep-water Earliest Oligocene Glacial Maximum (EOGM) in South Atlantic. *Chinese Science Bulletin* **49**, 2190–7.

Zijderveld, J. D. A. 1967. AC demagnetization rocks: Analyses of results. In *Methods in Paleomagnetism* (eds D. W. Collinson, K. M. Creer & S. K. Runcorn), pp. 254–86. Amsterdam, Netherlands: Elsevier Scientific.

Zouhri, S., Gingerich, P. D., El Boudali, N., Sebti, S., Noubhani, A., Rahali, M. & Meslouh, S. 2014. New marine mammal faunas (Cetacea and Sirenia) and sea level change in the Samlat Formation, upper Eocene, near Ad-Dakhla in southwestern Morocco. *Comptes Rendus Palevol* **13**, 599–610.

https://doi.org/10.1017/S0016756817000851 Published online by Cambridge University Press